ECS Transactions, 77 (10) 93-108 (2017)
10.1149/07710.0093ecst ©The Electrochemical Society

Towards an Improved Understanding of Electrochemical Oxygen Exchange Reactions on Mixed Conducting Oxides

J. Fleig, G. M. Rupp, A. Nenning, A. Schmid

Institute of Chemical Technologies and Analytics, TU Wien, 1060 Vienna, Austria

In solid oxide fuel cells or electrolysis cells with ionic and electronic conducting electrodes, the electrochemical reactions take place at the gas/solid interface of the mixed conducting electrode. This is in contrast to the situation met in aqueous electrolytes, where the reactions occur at the electrode/electrolyte interface. Thus, modified concepts are required to describe the reaction rates of such reactions on mixed conducting oxides. Here, it is discussed how overpotential and gas partial pressure affect reaction rates. A rate equation is suggested that also includes defects and the meaning of the empirical reaction orders is illustrated. Three experiments are presented that emphasize different aspects required for a mechanistic understanding of such reactions: A simultaneous variation of overpotential and partial pressure reveals the role of defects in oxygen evolution on $(La,Sr)FeO_{3-\delta}$ electrodes. Bias dependent impedance measurements with an analysis of the chemical capacitance gives information on the concentration of minority defects in $Sr(Ti,Fe)O_{3-\delta}$. Modification of $(La,Sr)CoO_{3-\delta}$ thin film surfaces by Sr or Co and impedance measurements in the pulsed laser deposition chamber help understanding catalytically active sites.

Introduction

An important goal of many electrochemical studies is to improve the mechanistic understanding of electrode reactions. From a knowledge of reaction pathways, rate limiting factors and mechanisms behind electrocatalysis, optimized electrodes can be suggested or designed. This is also true for the electrode reactions taking place in fuel cells and water electrolysis cells. However, the reaction mechanisms of oxygen reduction/evolution and hydrogen oxidation or water splitting strongly depend on the electrolyte used in the electrochemical cells and thus also the status of knowledge may be rather different for different electrolytes. In general, most information is available for electrochemical reactions in aqueous solutions. Hydrogen oxidation or evolution from aqueous solutions, for example, are rather well understood mechanistically.

Also for reactions on solid oxide electrolytes such as yttria stabilized zirconia (YSZ) there is general agreement on several mechanistic aspects, for example on the existence of two reaction paths (1-3): In one reaction path, only the electrode surface close to the triple phase boundary is electrochemically relevant (surface path). In a second path the redox reaction takes place at extended parts of the electrode surface and ions are supplied to the reaction sites through the electrode bulk. This second pathway (bulk path) requires

Downloaded on 2017-07-11 to IP 128.130.254.33 address. Redistribution subject to ECS terms of use (see ecsdl.org/site/terms_use) unless CC License in place (see abstract).

mixed ionic and electronic conductors (MIECs) as electrodes. Modifications of these paths are possible, e.g. with (atomic) gas diffusion through metal electrodes such as Ag (4) and Pt (5) or a surface path with the electrolyte surface rather than the electrode surface being the place of the redox reaction due to electron supply from the electrolyte (ceria under reducing conditions (6)).

For a predominant bulk path with oxygen exchange on the surface of the mixed conducting electrode, it is often well-known under which conditions the surface reaction or the ion (or electron) transport in the electrode is rate limiting. Moreover separation of the ion transfer resistance at the electrode/electrolyte interface from the resistance due to the redox reaction at the surface is often possible (7). However, regarding the understanding of the actual electrochemical redox reaction at the surface of the electrode, solid state electrochemistry still lacks behind electrochemistry in aqueous solutions. This is true for all kinds of "electrochemical oxygen exchange reactions", i.e. for oxygen reduction/evolution and hydrogen oxidation/water splitting.

In this paper, several aspects of this oxygen exchange on mixed conducting oxide electrodes are considered. First it is discussed what makes oxygen exchange on MIECs so different from the related reactions in aqueous systems. This also clarifies why even models for describing the (rarely measured) current-overpotential curves of the oxygen exchange reactions are not readily available. An approach for understanding reaction orders of these reactions is suggested. In the second part, three examples illustrate important factors affecting current voltage curves. Experiments show, how one can measure and analyze partial pressure dependent current voltage curves, how one may gain knowledge of the MIEC defect chemistry of polarized electrodes, and how additional information on the relation between surface chemistry and reaction rates can be obtained.

The Complexity of I-η Relations Describing Oxygen Exchange at MIEC Surfaces

Fundamental Difference between Electrochemical Reactions at MIEC Surfaces and Electrode/Electrolyte Interfaces

Fig. 1 sketches oxygen reduction taking place at a metal electrode in aqueous solution (a) and at a MIEC electrode on a solid electrolyte, e.g. YSZ (b). Several differences are of importance: The reaction in water takes place at temperatures mostly below 100°C while solid oxide fuel cells usually operate at temperatures well above 500°C (even though also at 300°C the reaction may take place at an easily measurable rate). The reacting species involved in the oxygen reduction reaction are different. This is already indicated by the different reaction equations: $O_2 + 4e^- + 4H_3O^+ \longleftrightarrow 6H_2O$ or $O_2 + 4e^- \longleftrightarrow 2O^{2-}$. Thus, also the exact reaction mechanism is different, with other intermediates being involved (e.g. OOH in water and possibly O_2^- for MIECs). However, the most severe difference is the fact that in water the reaction takes place at the electrode/electrolyte interface, while for a MIEC on YSZ the reaction occurs at the MIEC surface, i.e. at the gas/MIEC interface.

Downloaded on 2017-07-11 to IP 128.130.254.33 address. Redistribution subject to ECS terms of use (see ecsdl.org/site/terms_use) unless CC License in place (see abstract).

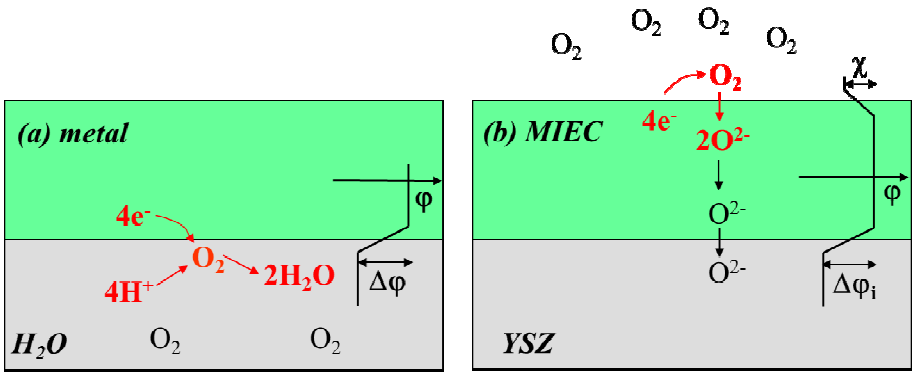

Figure 1. (a) Sketch of the oxygen reduction reaction at a metal electrolyte interface with the relevant and controllable electrostatic potential step $\Delta\varphi$ at this interface. (b) Sketch of the oxygen reduction on a MIEC surface with unknown and hardly controllable surface potential step χ, for example caused by charged adsorbates. The interfacial potential step $\Delta\varphi_i$ still exists, but does not affect the decisive reduction reaction kinetics at the surface.

Therefore, the external driving force of any net current (I) affects the reaction rates in different manners, and models for quantifying current-voltage relationships have to be different. A net reaction rate requires a difference between forward and backward reaction rates and thus deviation from equilibrium. This deviation is caused by a deviation of the electron electrochemical potential ($\tilde{\mu}_e$) in the electrode from its equilibrium (I=0) value, i.e. $\Delta\tilde{\mu}_e = \tilde{\mu}_e - \tilde{\mu}_e^{I=0} \neq 0$. The electrode overpotential η is given by $\Delta\tilde{\mu}_e$ via

$$\eta = -\frac{\Delta\tilde{\mu}_e}{F} \qquad [1]$$

For aqueous systems with the reaction at the electrode/electrolyte interface, this overpotential directly translates to a change of the electrostatic potential step $\Delta\varphi$ present at this interface, i.e. to $\eta = \Delta\varphi - \Delta\varphi^{I=0}$. Here and in the following $\Delta\varphi$ always refers to an electrostatic potential difference in space (across interfaces, e.g. $\Delta\varphi_i = \varphi_{MIEC} - \varphi_{YSZ}$) while $\Delta\tilde{\mu}, \Delta\mu$ indicate local deviations of electrochemical or chemical potentials from their equilibrium value under open circuit. Based on the direct electrostatic effect of η, a detailed mechanistic discussion of the electrochemical kinetics becomes possible for metal/H_2O interfaces, with rate limiting charge transfer being characterized by the so-called Butler-Volmer equation with both forward and backward reaction rates depending exponentially on the overpotential. In MIEC electrodes, the applied overpotential (i.e. a change of the electron electrochemical potential) does not affect the reaction in such a straightforward electrostatic manner. This is detailed in the following.

Effects of the Overpotential in MIECs

For the sake of simplicity let us assume that the only slow process of the overall oxygen reduction reaction in Figure 1b is the surface exchange reaction. Hence, the entire driving

Downloaded on 2017-07-11 to IP 128.130.254.33 address. Redistribution subject to ECS terms of use (see ecsdl.org/site/terms_use) unless CC License in place (see abstract).

force is used to get this surface reaction out of equilibrium and all other reaction steps in Figure 1b do not require severe deviation from equilibrium for sustaining a current. More specific, all charge transport processes in the MIEC are assumed to be fast, due to sufficiently high ionic and electronic conductivities, and thus $\Delta\tilde{\mu}_e$ is homogeneous in the entire MIEC electrode. Moreover, ion transfer at the MIEC/electrolyte interface is fast and the corresponding interface is in local equilibrium. Accordingly, the step of the chemical potential of oxide ions $\mu_{O^{2-},MIEC} - \mu_{O^{2-},YSZ}$ is counterbalanced by a local electrostatic potential step $\Delta\varphi_i$ such that the electrochemical potential of oxide ions is constant across the interface. We thus get

$$\Delta\varphi_i = \frac{\mu_{O^{2-},MIEC} - \mu_{O^{2-},YSZ}}{2F} . \qquad [2]$$

Even in such a simplified system the overpotential may change the forward and backward rates of the surface oxygen exchange in several different ways:

i) *Effect on $\Delta\chi$:* An electrostatic potential step might be present at the surface ($\chi = \varphi_{MIEC} - \varphi_{ad}$), e.g. due to a surface dipole layer caused by some charged adsorbates with electrostatic potential φ_{ad}. Also reducible surface cations can contribute to the surface dipole layer. This surface potential step depends on the applied overpotential in a very non-trivial manner: As detailed in Ref. (8), upon current flow the concentration of charged adsorbates may change and this causes a change of χ. Depending on the rate limiting step of the reaction and the adsorbate concentration, the surface potential change

$$\Delta\chi = \chi - \chi^{I=0} \qquad [3]$$

may be as high as 4η but can also be almost zero and the $\Delta\chi(\eta)$ relation may even vary with η (8). Since $\Delta\chi$ enters the equations of reaction rates (see below), current voltage relations may thus severely deviate from a simple Butler-Volmer type equation (8).

ii) *Effect on defect concentrations:* For a better mechanistic understanding of the oxygen exchange reactions it is often advantageous to take into account that ionic and electronic defects are the kinetically relevant charged "particles" in MIECs. Ionic defects are mostly oxygen vacancies, as for example in perovskite-type oxides such as $(La,Sr)(Co,Fe)O_{3-\delta}$. Electronic defects in semiconducting MIECs are electrons in the conduction band and holes in the valence band or the corresponding polarons. A change of $\tilde{\mu}_e$ and thus of the overpotential affects these defect concentrations, which becomes clear from the following consideration. The electrochemical potential of O^{2-} ($\tilde{\mu}_{O^{2-},MIEC}$) and the chemical potential of oxygen in the MIEC $\mu_{O,MIEC}$ are related by

$$\tilde{\mu}_{O^{2-},MIEC} - 2\tilde{\mu}_{e,MIEC} = \mu_{O,MIEC} . \qquad [4]$$

The MIEC/YSZ interface is assumed to be in local equilibrium even for applied overpotential and without loss of generality this can also be assumed for the entire

Downloaded on 2017-07-11 to IP 128.130.254.33 address. Redistribution subject to ECS terms of use (see ecsdl.org/site/terms_use) unless CC License in place (see abstract).

electrolyte and the reference electrode (or counter electrode). Therefore, $\Delta\tilde{\mu}_{O^{2-},MIEC} = 0$ holds also under current flow and we obtain from Eqs. 1 and 4

$$2\Delta\tilde{\mu}_{e,MIEC} = -2F\eta = -\Delta\mu_{O,MIEC}\,. \qquad [5]$$

This shows that the overpotential changes the chemical potential of oxygen in the MIEC and thus defect concentrations. This defect variation by overpotential is analogous to that caused by a variation of the external oxygen partial pressure (pO_2). The corresponding dependence of defect concentrations on the oxygen chemical potential μ_O is often illustrated in so-called Brouwer diagrams (log(concentration) versus log(pO_2)) and it does not play a role whether the oxygen partial pressure is a true gas pressure or an equivalent partial pressure in the MIEC defined by $\mu_{O,MIEC}$.

iii) *Effect on catalytic sites:* A third, less obvious effect of the voltage is via active reaction sites with special chemical properties, e.g. special adsorption sites leading to a certain bonding to the oxygen molecule or intermediate species that facilitates charge transfer or dissociation. The chemical nature of such active sites may be affected by the chemical potential of electrons in the MIEC and thus by the overpotential. Moreover, if cations with localized electronic charges (polarons) or oxygen vacancies are part of these active sites, their concentration may change with overpotential. Electrons trapped in oxygen vacancies may also be of relevance (particularly in reducing atmosphere) and their concentration may also change with overpotential. However, this possible effect of η is not further considered in this paper.

Location of the Electrostatic Potential Step η

It was already mentioned above that the electrostatic potential step at the electrochemically relevant surface is generally not equivalent to the applied overpotential η. However, between a metallic current collector used to apply the overpotential and the counter electrode, such an electrostatic potential difference has to exist upon current flow. It is helpful (though kinetically not essential) to understand the location of this electrostatic potential step. The oxygen chemical potential change due to an overpotential can be described in terms of defects by

$$\Delta\mu_{O,MIEC} = -\Delta\mu_{V,MIEC} + 2\Delta\mu_{h,MIEC} = 2F\eta \qquad [6]$$

with $\mu_{V,MIEC}, \mu_{h,MIEC}$ being the chemical potentials of vacancies and holes, respectively. For typical semiconducting perovskite type oxides such as (La,Sr)$FeO_{3-\delta}$ (LSF) or (La,Sr)$MnO_{3-\delta}$ (LSM) high oxygen partial pressures lead to predominant hole compensation of acceptor doping (9). In such a case, μ_O hardly affects the hole concentration and we find $\Delta\mu_{h,MIEC} \approx 0$. In other words, the entire change of the electrochemical potential of electrons $\tilde{\mu}_{e,MIEC} = -\mu_{h,MIEC} - F\varphi_{MIEC}$ is realized by a change of the electrostatic potential φ_{MIEC}.

Moreover,

Downloaded on 2017-07-11 to IP 128.130.254.33 address. Redistribution subject to ECS terms of use (see ecsdl.org/site/terms_use) unless CC License in place (see abstract).

$$\Delta\mu_{V,MIEC} \approx -\Delta\mu_{O,MIEC} = -2F\eta \qquad [7]$$

results from Eqs. 5 and 6, which means that the vacancy concentration drastically changes under polarization, as exemplified for LSM (10). This has a consequence at the MIEC/electrolyte interface: From Eqs. 2 and 7 we can conclude that the local electrostatic potential step at the MIEC/YSZ interface changes according to $\Delta\varphi_i = \Delta\varphi_i^{I=0} + \eta$, see Figure 2 (a). However, please note, that despite the apparently identical effect of the overpotential on $\Delta\varphi_i$ we are far from the situation met in aqueous electrolytes: There, the interfacial reaction is out of equilibrium, while for the MIEC/YSZ interface the corresponding interfacial charge transfer is still in local equilibrium and does not limit the reaction rate.

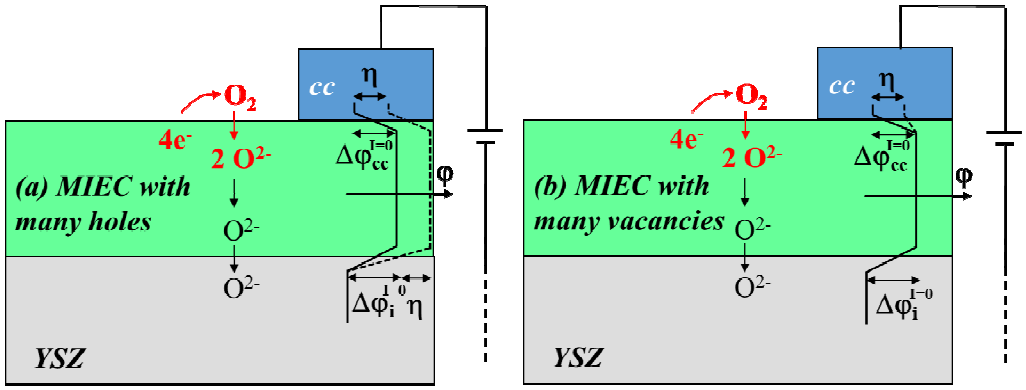

Figure 2. Sketches of the electrostatic potential steps in polarized MIEC electrodes. (a) In a MIEC with hole compensation of the acceptor dopant, the overpotential modifies the step at the MIEC/electrolyte interface. (b) For vacancy compensation, e.g. at low oxygen partial pressures, the corresponding electrostatic potential change takes place at the metallic current collector (cc)/MIEC interface. However, in both cases the corresponding interfaces are still in local equilibrium.

We may also consider the situation found in many acceptor-doped oxides under lower oxygen partial pressures (reducing conditions). Then, the acceptor doping is largely counter-balanced by oxygen vacancies. Hence, we get $\Delta\mu_{V,MIEC} \approx 0$ and from Eqs. 5 and 6

$$\Delta\mu_{h,MIEC} \approx \frac{1}{2}\Delta\mu_{O,MIEC} = F\eta\,. \qquad [8]$$

Now, the entire overpotential or $\Delta\tilde{\mu}_e$ translates to a chemical potential change of electrons and thus a severe change of the electronic defect concentrations. This also means that the chemical potential of ions in the MIEC as well as the electrostatic potential in the MIEC remain unaffected. Therefore, the MIEC/electrolyte interfacial potential step stays at its equilibrium value ($\Delta\varphi_i \approx \Delta\varphi_i^{I=0}$), despite applied overpotential. The unavoidable electrostatic potential step under voltage can now be found at the current collector/MIEC interface. There, anyway another interfacial potential step $\Delta\varphi_{cc}$ is

Downloaded on 2017-07-11 to IP 128.130.254.33 address. Redistribution subject to ECS terms of use (see ecsdl.org/site/terms_use) unless CC License in place (see abstract).

present, due to a difference of μ_e in MIEC and current collector, and this $\Delta\varphi_{cc}$ is then changed by η, due to the change of $\mu_{e,MIEC}$. This is sketched in Figure 2 (b).

A Modified Approach to Understand I-η Relations of Oxygen Exchange

In DC experiments of surface oxygen exchange one may measure the current for different overpotentials and gas partial pressures p, thus obtaining empirical I(η,p) relations; in H_2/H_2O even two partial pressures are involved. However, it is non-trivial to interpret these curves in terms of reaction mechanisms. This is due to the numerous effects of the overpotential, see above, and also of the partial pressure. The latter affects concentrations of adsorbed species, and thus reactant concentrations and surface potential steps, as well as defect concentrations in the MIEC. In Ref. (8), I-η relations and partial pressure dependences were calculated for several kinetic situations and one may consider a large number of mechanistic models and compare their predicted gas and overpotential dependences with the measured ones. However, in order to interpret measured I(η,p) curves in terms of possible reaction mechanisms, it may be advantageous to first get an idea on the role of defect concentrations. This requires a formulation of reaction rates such that the defect concentrations and their reaction order become obvious.

Here, we suggest such an approach for quantifying reaction rates of oxygen exchange reactions by considering defect concentrations in an explicit manner. Electronic defects can be formulated either with electrons in the conduction band or with holes in the valence band of a semiconducting MIEC, e.g. $(La,Sr)FeO_{3-\delta}$ or $Sr(Ti,Fe)O_{3-\delta}$. Accordingly, we have to deal with the oxygen reduction and evolution reactions

$$\text{forward: } O_2 + 4e' + 2V_O^{\bullet\bullet} \rightarrow 4O_O^x \quad \text{or} \quad O_2 + 2V_O^{\bullet\bullet} \rightarrow 4O_O^x + 4h^{\bullet} \qquad [9]$$

$$\text{backward: } 4O_O^x \rightarrow O_2 + 4e' + 2V_O^{\bullet\bullet} \quad \text{or} \quad 4O_O^x + 4h^{\bullet} \rightarrow O_2 + 2V_O^{\bullet\bullet} \qquad [10]$$

and with the water splitting and hydrogen oxidation reactions

$$\text{forward: } H_2O + 2e' + V_O^{\bullet\bullet} \rightarrow O_O^x + H_2 \quad \text{or} \quad H_2O + V_O^{\bullet\bullet} \rightarrow O_O^x + H_2 + 2h^{\bullet} \qquad [11]$$

$$\text{backward: } O_O^x + H_2 \rightarrow H_2O + 2e' + V_O^{\bullet\bullet} \quad \text{or} \quad O_O^x + H_2 + 2h^{\bullet} \rightarrow H_2O + V_O^{\bullet\bullet} \qquad [12]$$

For describing current densities of these forward (reduction) or backward (oxidation) reactions we suggest the general relation

$$j = j^* \cdot c_d^{\nu_d} \cdot p^{\nu_p} \cdot e^{\alpha' F \chi^{I=0}/RT} \cdot c_{cat} \cdot e^{\alpha F \Delta\chi/RT} \qquad [13]$$

or, more specific, for reduction with negative current densities

$$\vec{j} = -\vec{j}^* \cdot \vec{c}_d^{\nu_{d,f}} \cdot \vec{p}^{\nu_{p,f}} \cdot e^{-\beta' F \chi^{I=0}/RT} \cdot \vec{c}_{cat} \cdot e^{-\beta F \Delta\chi/RT} \qquad [14]$$

and for oxidation

Downloaded on 2017-07-11 to IP 128.130.254.33 address. Redistribution subject to ECS terms of use (see ecsdl.org/site/terms_use) unless CC License in place (see abstract).

$$\overleftarrow{j} = \overleftarrow{j}^{*} \cdot \bar{c}_d^{\nu_{d,b}} \cdot \bar{p}^{\nu_{p,b}} \cdot e^{\alpha' F \chi^{I=0}/RT} \cdot \bar{c}_{cat} \cdot e^{\alpha F \Delta\chi/RT} . \qquad [15]$$

The sum of Eqs. 14 and 15 gives the measurable net current density; f and b in the exponents denote forward and backward, respectively. In accordance with the reactions 9-12 we consider normalized defect c_d and gas concentrations p in the rate equations.

The defect concentration factor $c_d^{\nu_d}$ represents all defects involved in the reaction and thus may often have to be replaced by the product of two different defect concentrations with different exponents. Defects may affect the reaction rates in two different ways. First, they may be reactants in the rate limiting step and thus their concentration affects the reaction rate in a direct manner. Second, charged intermediate species such as $O_{2,ad}^-$ or O_{ad}^- may be involved in the rate limiting step and their equilibrium concentrations can be indirectly affected by defect concentrations (hole, electrons) via mass action laws of charge transfer reactions before or after the rate limiting step. Hence, the reaction orders ν_d includes direct and indirect concentration dependences. For example, if the transfer of an electron in the conduction band to an adsorbed oxygen intermediate is the rate limiting step of the reaction, e.g. $O_{2,ad}^- + e' \rightarrow 2O_{ad}^-$, $\nu_{e,f}$=1 would result for a direct effect of the electrons only. However, the $O_{2,ad}^-$ intermediate concentration is given by the mass action law of the reaction $O_{2,gas} + e' \rightarrow O_{2,ad}^-$ and this reaction also includes electrons. This causes an additional indirect effect of electrons in the reaction order and in a dilute case we find $\nu_{e,f} = 2$.

The second concentration factor refers to the normalized gas partial pressure p. Again, this may have to be replaced by a product, if two gases are relevant. With few exceptions (e.g. rate limiting adsorption) gas molecules do not enter the rate limiting step in a direct manner. However, the partial pressures affect the concentrations of surface adsorbates and those can be involved in the rate limiting step. Thus, the concentration factor p^{ν_p} is possibly due to an indirect effect via mass action laws.

A second indirect effect of the oxygen partial pressure exists due to the surface potential χ. The surface potential varies with varying concentration of charged surface adsorbates and thus depends on the oxygen partial pressure. This is shown in Ref. (11) for several examples based on calculations including electrostatic repulsion of charged adsorbates and site restriction. The partial pressure dependent $\chi^{I=0}$ affects all mass action constants of charge transfer reactions and this is taken into account by the first exponential factor in Eq. 13, $e^{\alpha' F \chi^{I=0}/RT}$. Factor α' (or β' in Eq. 14) depends on the charge of the intermediate species. Nominally, it would also be possible to include this factor into the p^{ν_p} factor with the partial pressure dependent exponent ν_p.

The third concentration factor c_{cat} considers the catalytically active sites. Those may be the "standard" defects such as oxygen vacancies or (localized) electrons, i.e. polarons and then their concentration is already included in the c_d factor and c_{cat} is not applicable. However, also other catalytically active sites are feasible, for example ad-atoms, kinks or

Downloaded on 2017-07-11 to IP 128.130.254.33 address. Redistribution subject to ECS terms of use (see ecsdl.org/site/terms_use) unless CC License in place (see abstract).

edges. Then we have to consider their concentration by an extra factor and we assume a linear dependence of the reaction rate on this active site concentration c_{cat}.

The last exponential factor in Eqs. 13-15 (with $\Delta\chi$) includes two effects of the surface potential change due to an applied overpotential; please note that $\Delta\chi$ is generally not equivalent with the overpotential η, see above. The deviation of χ from its equilibrium value directly affects the reaction rate of any rate limiting charge transfer by an exponential factor which includes fractions α'' or β'' of $\Delta\chi$ for oxidation and reduction reactions. For an electron transfer α'' corresponds to the well-known symmetry factor with $\beta'' = 1 - \alpha''$. However, there is also an indirect effect of $\Delta\chi$, namely via a further change of mass action constants of all fast charge transfer reactions, see above. Hence, this factor also includes the non-equilibrium extension of the other exponential factor with $\alpha'\chi^{I=0}$. We get $\alpha = \alpha' + \alpha''$ and $\beta = \beta' + \beta''$ and in general $\beta \neq 1\text{-}\alpha$. The prefactors j^*, finally, describe the reaction rates for standard concentrations and absence of any χ.

All together the overpotential affects the rate equations 13-15 primarily via $c_d(\eta)$ and by $\Delta\chi(\eta)$. The effect of the partial pressure is split into three factors, the effect on defects ($c_d^{\nu_d}$ -factor), on adsorbates (p^{ν_p} -factor) and on the surface potential step $\chi^{I=0}$ (Furthermore the partial pressure affects the $\Delta\chi$–η relation). One advantage or our new equations is the fact that we can separate defect chemical effects of partial pressure or overpotential from other effects of these experimental parameters.

In the next section we show exemplarily, which types of experiments may help to further analyze this complex situation. Please note, that these experiments are not yet performed on one and the same system but on Sr-doped $LaFeO_3$ (I-η curves), Fe-doped $SrTiO_3$ (chemical capacitance measurements) and Sr-doped $LaCoO_3$ (in-situ impedance PLD). In future, measurements on the same electrodes may reveal a more complete picture of the kinetics of oxygen exchange on MIECs.

Experiments for Understanding Oxygen Exchange Reactions on MIEC Surfaces

Current-Overpotential Curves Measured on Sr-doped $LaFeO_3$ (LSF)

Owing to several reasons, it is not straightforward to measure the I-η characteristics of oxygen exchange reactions. First, the effect of the counter electrode has to be eliminated. This may be done by three point measurement, but a proper location of the reference electrode is often non-trivial in solid oxide cells (12-14). Another possibility is the use of working electrodes with much larger electrode resistances than the counter electrode, e.g. by using microelectrodes as working electrodes (15). Still, it may be difficult to warrant absence of any counter electrode resistance for a large bias voltage range, especially for working electrodes with exponentially increasing currents under load. For an analysis of the current-voltage behavior of the surface reaction on MIECs also absence of any transport resistance in the electrode is essential. This is often not the case for porous MIEC electrodes, where models such as the ALS model (16) describe the interplay of both surface reaction and transport and the importance of each depends on the location within the electrode.

Downloaded on 2017-07-11 to IP 128.130.254.33 address. Redistribution subject to ECS terms of use (see ecsdl.org/site/terms_use) unless CC License in place (see abstract).

Here, I(η,p) curves of the oxygen evolution reaction were measured on $La_{0.6}Sr_{0.4}FeO_{3-\delta}$ (LSF) thin film electrodes prepared by pulsed laser deposition on an yttria stabilized zirconia (YSZ) single crystal. An additional Pt thin film grid was deposited beneath the LSF layer to warrant negligible in-plane electronic resistances. At the outer rim of the quadratic YSZ single crystal a reference electrode was deposited, consisting of a Pt wire and LSF paste. From impedance measurements, the ohmic resistance R_{ohm} between LSF working electrode and reference electrode was determined and thus the electrode overpotential could be calculated from the applied voltage U and the measured current I by $\eta = U - R_{ohm}I$. From additional measurements we know that electron and ion transport in the film does not affect the results and that the interfacial charge transfer from LSF into YSZ is sufficiently fast.

Figure 3a displays current voltage curves measured at 600°C in different oxygen atmospheres (0.25 mbar, 1 mbar, 5 mbar oxygen in nitrogen). These net currents represent the difference between forward (reduction) and backward (oxidation) current and for small overpotentials certainly both reactions contribute to the measured current. However, most probably the oxygen reduction reaction is suppressed by larger positive overpotentials and we may safely assume that the measured currents largely reflect the backward reaction of oxygen evolution. This backward current clearly depends on the oxygen partial pressure and increases the more oxygen is present. At first sight one may conclude that gas molecules accelerate oxygen evolution.

This, however, is a wrong interpretation. Alternatively, we may plot the same currents versus the chemical potential of oxygen in the MIEC or the oxygen potential η_{eff} defined by

$$\eta_{eff} = \frac{1}{2F}\left(\mu_{O.MIEC} - \mu_{O,ref}\right). \qquad [16]$$

Together with Eq. 5 and $\Delta\mu_{O,MIEC} = \mu_{O,MIEC} - \mu_{O,MIEC}^{I=0} = \mu_{O,MIEC} - \mu_{O,gas}$ we get

$$\eta_{eff} = \eta + \frac{1}{2F}\left(\mu_{O,gas} - \mu_{O,ref}\right) = \eta + \frac{RT}{4F}\ln\left(\frac{p_{O2,gas}}{1\,bar}\right) \qquad [17]$$

Here $\mu_{O,ref}$ denotes the oxygen chemical potential corresponding to 1 bar O_2 and $p_{O2,gas}$ is the oxygen partial pressure in the gas phase. The corresponding plot in Fig. 3b thus shows the oxygen evolution current in dependence of the defect chemical state given by η_{eff}. Now we can compare the oxygen evolution for identical defect concentrations in LSF but different oxygen partial pressures outside. Obviously, the oxygen evolution current only depends on the oxygen potential of LSF. For identical μ_O the gas has no further effect and in Eq. 15 $\nu_{p,b} = 0$; adsorbed oxygen does not promote oxygen evolution. A further increase of the oxygen partial pressures (not shown) leads to an additional effect of the gas phase and thus to $\nu_{p,b} \neq 0$. For oxygen evolution, holes are the only defect required and the hole concentration in the valence band increases with increasing oxygen chemical potential. This is in agreement with the measured increase of the current

Downloaded on 2017-07-11 to IP 128.130.254.33 address. Redistribution subject to ECS terms of use (see ecsdl.org/site/terms_use) unless CC License in place (see abstract).

with oxygen chemical potential. A more quantitative analysis of the hole related exponent $\nu_{h,b}$ and of the slope of the log(I)-η curve, however, is beyond the scope of this paper.

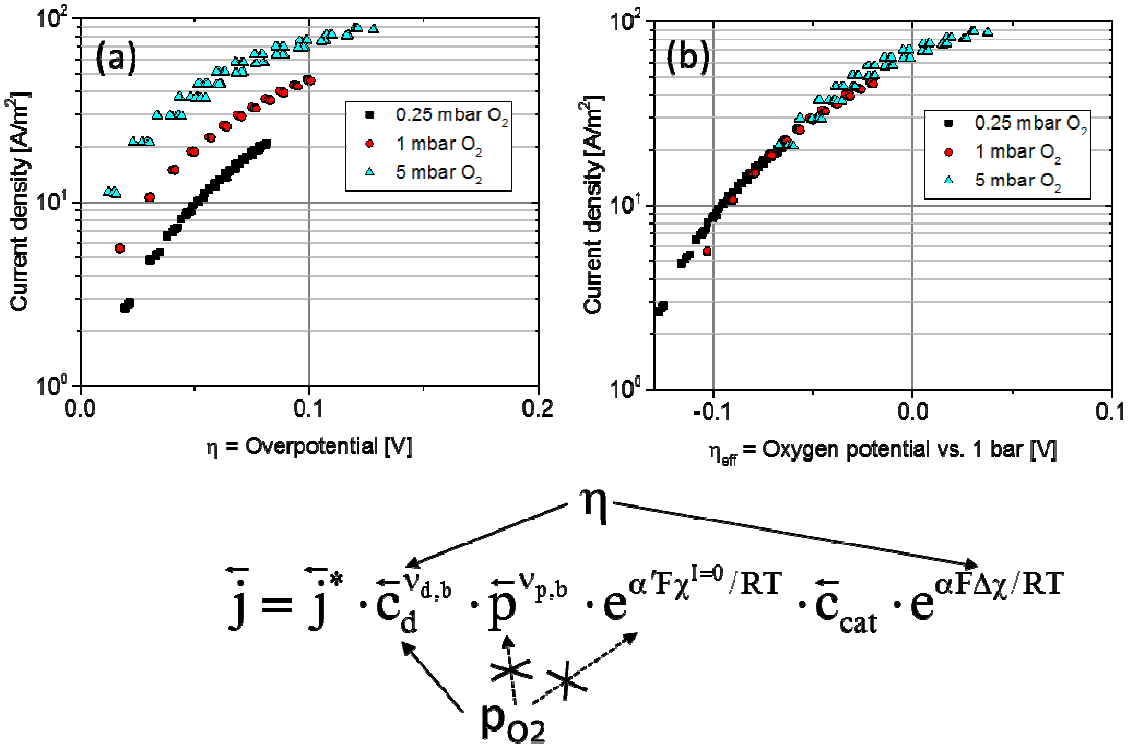

Figure 3. (a) Current-overpotential curves measured for a LSF thin film electrode on YSZ at 600°C. The oxygen partial pressure affects the current at given overpotential. However, the curves are simply shifted by a factor (RT/4F)ln(p_2/p_1). (b) Current-oxygen potential curves, indicating that for the same oxygen potential in the MIEC the same oxygen evolution current results. The formula at the bottom summarizes the main ways how oxygen partial pressure and overpotential affect the backward reaction rate and also indicates that here p_{O2} only changes the defect chemical state.

Overpotential Dependence of the Chemical Capacitance of Fe-doped $SrTiO_{3-\delta}$ (STF)

This analysis of a current-overpotential curve shows that defect concentrations can strongly affect reaction rates; this was also concluded in many earlier papers, for example suggesting the concentration of oxygen vacancies (17) or electrons (18) as being highly relevant in oxygen reduction. However, analyzing the reaction orders of defects, ν_d, is far from trivial since any change of the defect concentration by partial pressure or overpotential also changes other factors, see above. Hence, it would be helpful to have complementary information on defects and their dependence on the oxygen chemical potential. For many materials, defect chemical models exist and allow calculation of defect concentrations for different chemical potentials and temperatures. Such models were often extracted from thermogravimetric studies and/or coulometric titration but also from conductivity studies.

Downloaded on 2017-07-11 to IP 128.130.254.33 address. Redistribution subject to ECS terms of use (see ecsdl.org/site/terms_use) unless CC License in place (see abstract).

Another tool for gaining information on defect concentration is hardly used yet. It is the measurement of the chemical capacitance. The chemical capacitance of an oxide (19) with sample volume V is defined by

$$C_{chem} = 4F^2 V n^0 \left(\frac{\partial \mu_O}{\partial c_O} \right)^{-1} \quad [18]$$

The key factor is the derivative of the oxygen chemical potential with respect to the normalized concentration of oxygen c_O. Here, normalization of the concentration is done with respect to the absolute concentration of oxygen sites n^0. Essentially, the chemical capacitance is proportional to the slope of a TGA curve. The chemical potential of oxygen can be expressed in terms of ionic and electronic defects (cf. Eq. 6). Moreover, a change of the oxygen (or vacancy) concentration c_V is related to a change of electronic charge carrier concentration c_{eon} by charge neutrality. Therefore, we can express C_{chem} also in terms of defect concentrations and for dilute defects we get (20)

$$C_{chem} = \frac{4F^2 V n^0}{RT} \frac{1}{\left(\frac{1}{c_V} + \frac{4}{c_{eon}} \right)}. \quad [19]$$

Accordingly, the minority defect determines the chemical capacitance and its concentration can be deduced from C_{chem}.

Since the chemical potential of oxygen can be modified by an overpotential, also the chemical capacitance should strongly depend on the overpotential and from such measurements information on defect concentrations under polarization can be gained. As an example, Figure 4 displays the chemical capacitance measured on a $SrTi_{0.7}Fe_{0.3}O_{3-\delta}$ microelectrode of 100 µm diameter (100 nm thickness) in strongly reducing atmosphere (25 mbar H_2 / 25 mbar H_2O) at 560°C. This chemical capacitance was determined from the main arc visible in impedance spectra (see e.g. Refs. (21, 22)). A very characteristic dependence on the overpotential is found. For negative overpotentials the chemical capacitance strongly increases while for positive η a minimum is reached and then the chemical capacitance again increases. This is in accordance with the defect chemical model of this material (23) where moderately low oxygen chemical potentials lead to an oxygen vacancy compensation of the Fe doping and holes as minority charge carriers. The hole concentration decreases until the intrinsic point is reached. Then electrons take over in C_{chem} and their concentration increases with decreasing oxygen chemical potential.

This shows that the chemical capacitance can give highly valuable information on defects and their dependence on the chemical potential or overpotential. In particular, C_{chem} is very sensitive to the minority defect concentrations. Another strength of this method is that by application of an overpotential we can gain information on the intermediate pO_2 regime, for which gas mixtures are hardly available. Performing bias dependent impedance studies during DC current-voltage measurements may thus reveal direct information on defect concentrations in the specific MIEC electrodes under investigation. However, such measurements are again not trivial. Either they employ microelectrodes and can thus suffer from problems of inhomogeneous heating in usual

Downloaded on 2017-07-11 to IP 128.130.254.33 address. Redistribution subject to ECS terms of use (see ecsdl.org/site/terms_use) unless CC License in place (see abstract).

set-ups (also in our measurement). Or three electrode measurements are used, which means that we not only have to cope with the problems of DC three point measurements (see above) but also with additional artefacts of three point AC measurements (12-14, 24, 25). It is also beyond the scope of our paper to give a detailed quantitative analysis of the curve in Figure 4.

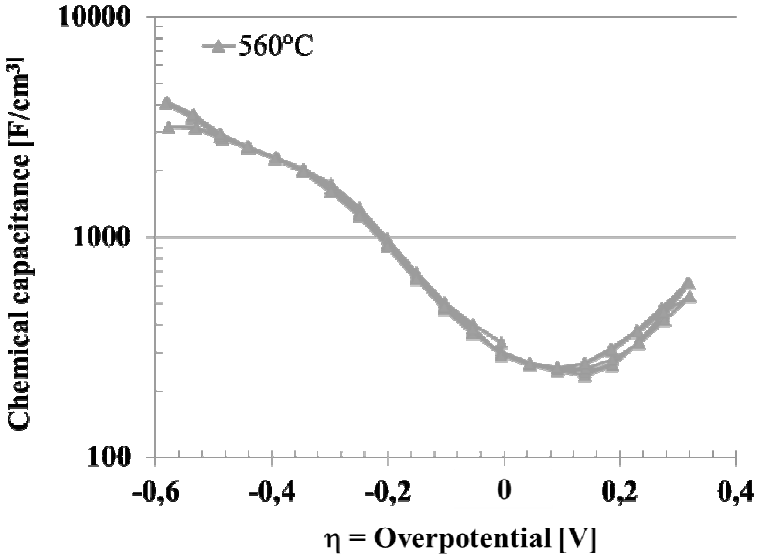

Figure 4. Chemical capacitance of a STF microelectrode measured in H_2/H_2O (1:1) mixture at 560°C.

Moreover, we have to take into account that, irrespective of the measurement method, usually bulk defect concentrations are determined, while it is the surface defect concentration which enters the reaction rate. Determination of surface defect concentrations is very non-trivial and little information is available so far. For ceria, for example, quantitative data exist (26) and those reveal that surfaces tend to be more reduced, i.e. have more oxygen vacancies and electrons but less holes. This was qualitatively confirmed for STF and LSF (27). Even if absolute defect concentrations of bulk and surface may be different, their chemical potential dependences might be similar and a first interpretation of I-η curves in terms of bulk defect concentrations can be helpful.

Modifying the Oxygen Exchange Resistance of Sr-doped $LaCoO_{3-\delta}$ (LSC) by Surface Decoration

Gaining reliable knowledge on the catalytically active sites and their concentrations is one of the most difficult parts of the analysis of electrochemical reactions on MIECs. In many studies, it was shown that the exact surface chemistry of MIECs may severely differ from the bulk composition and that this has a strong impact on the oxygen exchange reaction. Among others, Sr segregation was found to take place and usually lowers the reaction rates (28-30). However, very defined and controlled changes of surfaces and subsequent analysis of the reaction rates are difficult to achieve.

Downloaded on 2017-07-11 to IP 128.130.254.33 address. Redistribution subject to ECS terms of use (see ecsdl.org/site/terms_use) unless CC License in place (see abstract).

We modified the reaction chamber of a pulsed laser deposition (PLD) set-up such that immediately after depositing material on a MIEC electrode its electrochemical properties can be measured in-situ by impedance spectroscopy. Figure 5a displays the change of impedance spectra when depositing Sr oxide onto a $La_{0.6}Sr_{0.4}CoO_{3-\delta}$ (LSC) electrode by applying 88 pulses on a single crystalline SrO target. These impedance measurements were performed at the partial pressure and temperature also used for PLD (0.5 mbar O_2 and 450°C). The surface modification corresponds to about one monolayer of SrO and drastically increases the oxygen exchange resistance of the LSC electrode (i.e. the size of the main arc visible in the impedance spectrum measured with the LSC thin film electrode on top of a YSZ single crystalline electrolyte substrate). This can be partly reversed by deposition of Co_3O_4, indicating that Co might be important for catalytically active sites. More details on such measurements will be given in a forthcoming paper.

Additional partial pressure dependent measurements of the oxygen exchange resistance (without applied bias voltage) are displayed in Figure 5b. Here, Co was directly deposited on an as prepared LSC electrode and this substantially decreased the oxygen exchange resistance. Nevertheless, similar slopes (in the range of -0.5) are found for both samples and this may indicate that the mechanism and the rate limiting step was not modified by Co. Hence, the active site concentration might be increased by Co deposition while the other factors in our rate equations remained the same. However, this is only a preliminary interpretation and requires additional measurements.

Please note that according to our model (Eqs. 13-15) the slope of -0.5 has not a simple meaning and does not necessarily imply that an atomic oxygen species is involved in the rate limiting step. Rather, this empirical reaction order $\nu_{p,emp}$ is a complex interplay of several partial pressure dependences: It may include the indirect oxygen partial pressure dependence of oxygen reduction via adsorbates ($\nu_{p,f}$) but also an effect on the defect concentrations of forward and backward reactions.

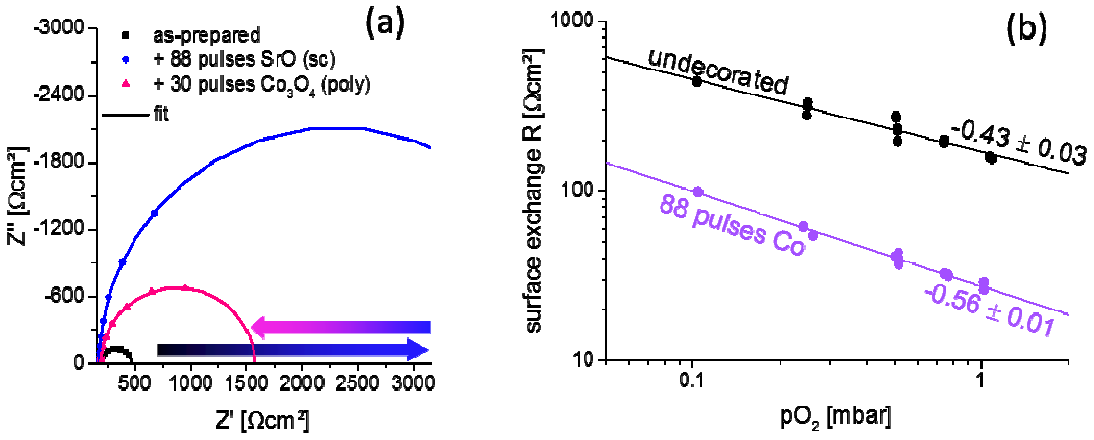

Figure 5. (a) Impedance spectra of an LSC thin film on a YSZ single crystal measured inside the PLD chamber at 450°C in 0.5 mbar O_2, as prepared, after depositing additional SrO (88 pulses) and after an additional deposition step using Co_3O_4 (30 pulses). (b) Surface oxygen exchange resistances deduced from such spectra in dependence of the oxygen partial pressure for an as-prepared sample and after Co_3O_4 decoration of the same sample.

Downloaded on 2017-07-11 to IP 128.130.254.33 address. Redistribution subject to ECS terms of use (see ecsdl.org/site/terms_use) unless CC License in place (see abstract).

Conclusions

For a better understanding of the kinetics of oxygen exchange reactions, a model was developed in which the defect concentrations explicitly enter the rate equations. It could be shown how the overpotential and the oxygen partial pressure as the main experimental parameters affect the individual factors in the rate equation. It became clear that the overpotential dependence as well as the partial pressure dependence of oxygen exchange rates can be highly non-trivial and a simple interpretation of empirical slopes or reaction orders can be highly misleading.

Moreover, three types of experiments are shown that may help understanding the reaction mechanism of oxygen exchange. Three point current voltage measurements with LSF thin film working electrodes make use of a defect chemical counterbalancing of gas phase and overpotential. This revealed the importance of the defect chemical state for oxygen evolution on these electrodes. Chemical capacitance measurements under different overpotentials gave information on minority defect concentrations of polarized STF electrodes. Finally, knowledge on active sites, their nature and their number are obtained from impedance measurements on LSC thin film electrodes, performed in the chamber used for pulsed laser deposition (PLD) immediately after surface modification.

Acknowledgments

The authors gratefully acknowledge funding by FWF (Austrian Science Fund) project P4509-N16.

References

1. S. B. Adler, *Chemical Reviews*, **104**, 4791 (2004).
2. J. Fleig, *Annual Review of Materials Research*, **33**, 361 (2003).
3. W. C. Chueh and S. M. Haile, in *Annual Review of Chemical and Biomolecular Engineering, Vol 3*, J. M. Prausnitz Editor, p. 313, Annual Reviews, Palo Alto (2012).
4. R. Jiménez, T. Kloidt and M. Kleitz, *J. Electrochem. Soc.*, **144**, 582 (1997).
5. A. K. Opitz, A. Lutz, M. Kubicek, F. Kubel, H. Hutter and J. Fleig, *Electrochimica Acta*, **56**, 9727 (2011).
6. W. C. Chueh, Y. Hao, W. Jung and S. M. Haile, *Nat. Mater.*, **11**, 155 (2012).
7. F. S. Baumann, J. Fleig, H. U. Habermeier and J. Maier, *Solid State Ionics*, **177**, 1071 (2006).
8. J. Fleig, *Phys. Chem. Chem. Phys.*, **7**, 2027 (2005).
9. M. Kuhn, S. Hashimoto, K. Sato, K. Yashiro and J. Mizusaki, *Solid State Ionics*, **195**, 7 (2011).
10. T. M. Huber, E. Navickas, G. Friedbacher, H. Hutter and J. Fleig, *ChemElectroChem*, **2**, 1487 (2015).
11. J. Fleig, R. Merkle and J. Maier, *Phys. Chem. Chem. Phys.*, **9**, 2713 (2007).
12. S. B. Adler, *J. Electrochem. Soc.*, **149** (2002).
13. G. Hsieh, T. O. Mason, E. J. Garboczi and L. R. Pederson, *Solid State Ionics*, **96**, 153 (1997).

Downloaded on 2017-07-11 to IP 128.130.254.33 address. Redistribution subject to ECS terms of use (see ecsdl.org/site/terms_use) unless CC License in place (see abstract).

14. J. Winkler, P. V. Hendriksen, N. Bonanos and M. Mogensen, *J. Electrochem. Soc.*, **145**, 1184 (1998).
15. J. Fleig, *Solid State Ionics*, **161**, 279 (2003).
16. S. B. Adler, J. A. Lane and B. C. H. Steele, *J. Electrochem. Soc.*, **144**, 1884 (1997).
17. L. Wang, R. Merkle, Y. A. Mastrikov, E. A. Kotomin and J. Maier, *J. Mater. Res.*, **27**, 2000 (2012).
18. W. Jung and H. L. Tuller, *Adv. Energy Mater.*, **1**, 1184 (2011).
19. J. Jamnik and J. Maier, *J. Electrochem. Soc.*, **146**, 4183 (1999).
20. J. Fleig, A. Schmid, G. M. Rupp, C. Slouka, E. Navickas, L. Andrejs, H. Hutter, L. Volgger and A. Nenning, *Acta Chim. Slov.*, **63**, 509 (2016).
21. G. M. Rupp, A. Schmid, A. Nenning and J. Fleig, *J. Electrochem. Soc.*, **163**, F564 (2016).
22. A. Nenning, A. K. Opitz, T. M. Huber and J. Fleig, *Phys. Chem. Chem. Phys.*, **16**, 22321 (2014).
23. M. Kuhn, J. J. Kim, S. R. Bishop and H. L. Tuller, *Chem. Mat.*, **25**, 2970 (2013).
24. G. Fafilek, *Solid State Ionics*, **176**, 2023 (2005).
25. G. Hsieh, S. J. Ford, T. O. Mason and L. R. Pederson, *Solid State Ionics*, **91**, 191 (1996).
26. W. C. Chueh, A. H. McDaniel, M. E. Grass, Y. Hao, N. Jabeen, Z. Liu, S. M. Haile, K. F. McCarty, H. Bluhm and F. El Gabaly, *Chem. Mat.*, **24**, 1876 (2012).
27. A. Nenning, A. K. Opitz, C. Rameshan, R. Rameshan, R. Blume, M. Havecker, A. Knop-Gericke, G. Rupprechter, B. Klotzer and J. Fleigt, *J. Phys. Chem. C*, **120**, 1461 (2016).
28. Y. Chen, W. Jung, Z. H. Cai, J. J. Kim, H. L. Tuller and B. Yildiz, *Energy Environ. Sci.*, **5**, 7979 (2012).
29. G. M. Rupp, A. Limbeck, M. Kubicek, A. Penn, M. Stoger-Pollach, G. Friedbacher and J. Fleig, *J. Mater. Chem. A*, **2**, 7099 (2014).
30. M. Kubicek, A. Limbeck, T. Fromling, H. Hutter and J. Fleig, *J. Electrochem. Soc.*, **158**, B727 (2011).

Downloaded on 2017-07-11 to IP 128.130.254.33 address. Redistribution subject to ECS terms of use (see ecsdl.org/site/terms_use) unless CC License in place (see abstract).